Materials Research Express

PAPER

Investigation on hot tearing behavior and its mechanism of Mg-4.5Zn-xY-yNd(x + y = 6, x = 0, 1, 3, 6) alloys

To cite this article: Xingxing Li *et al* 2019 *Mater. Res. Express* **6** 106535

Materials Research Express

CrossMark

RECEIVED
4 July 2019

REVISED
27 July 2019

ACCEPTED FOR PUBLICATION
2 August 2019

PUBLISHED
9 August 2019

PAPER

Investigation on hot tearing behavior and its mechanism of Mg-4.5Zn-xY-yNd(x + y = 6, x = 0, 1, 3, 6) alloys

Xingxing Li[1], Zheng Liu[1], Yue Wang[1], Ziqi Wei[1], Shimeng Liu[1], Zhenglai Zhang[2] and Yingdong Ju[3]

[1] College of Materials Science and Engineering, Shenyang University of Technology, Shenyang, People's Republic of China
[2] Zhejiang Huashuo Technology Co., Ltd, Ningbo 315802, People's Republic of China
[3] Ningbo Haizhi Institute of Materials Industry Innovation, Ningbo 315033, People's Republic of China

E-mail: zliu4321@126.com

Keywords: Mg-Zn-Y-Nd alloy, hot tearing susceptibility, LPSO phase, W-phase, T-phase

Abstract

The hot tearing susceptibility (HTS) and its mechanism of Mg-4.5Zn-xY-yNd (x + y = 6, x = 0, 1, 3, 6) alloys is studied based on Clyne-Davies' model and 'T' mold. The hot tearing tendency of four alloys is characterized by SEM, XRD and TEM. Morever, HTS of four kinds of Mg-4.5Zn-xY-yNd alloys is predicted by numerical simulation (ProCAST). The order of the four alloys arranged according to HTS from high to low is as follows: Mg-4.5Zn-3Y-3Nd > Mg-4.5Zn-1Y-5Nd > Mg-4.5Zn-6Nd > Mg-4.5Zn-6Y. The results show that the crystalline state of α-Mg phase and the type of the second phase change with the relative contents of Y and Nd, which are the main factors determining the hot tearing tendency. For Mg-4.5Zn-6Y alloy, the main precipitated phases are LPSO phase ($Mg_{12}ZnY$) and W phase ($Mg_3Zn_3Y_2$). For Mg-4.5Zn-3Y-3Nd and Mg-4.5Zn-1Y-5Nd alloys, the main precipitates are W phase ($Mg_3Zn_3(Y, Nd)_2$). For Mg-4.5Zn-6Nd alloy, the main precipitation phase is only T phase (Mg-Zn-Nd ternary phase).

1. Introduction

With the shortage of global energy and resources, countries around the world are paying more attention to environmental protection. Magnesium alloys have many advantages, such as less melting energy consumption, faster feeding and solidification speed, shorter die casting cycle and longer service life of mold. The effect of substituting steels, aluminium alloys and plastic parts under conventional use conditions is very excellent. Therefore, it is known as 'Metal of the 21st Century' and widely used in automobile, computer, communication and other broad fields [1–4].

Due to the low mechanical properties of commercial magnesium alloys, the development of new magnesium alloys with high strength and toughness has become a new research hot focus. Previous studies have shown that the mechanical properties of magnesium alloys can be significantly improved by adding appropriate rare earth [5–16]. Li *et al* [17] found that the yield strength, tensile strength and elongation of Mg-Zn alloys with Nd (Mg-0.2Zn-3Nd-0.4Zr) are 119 MPa, 186.7 MPa and 10.04% respectively. After aging at 200°C for 16 hours, the yield strength and tensile strength increased to 140 MPa and 250 MPa, respectively. Chen *et al* [18] found that the tensile strength and yield strength of Mg-Zn-Nd alloy with Y (Mg-0.2Zn-6Y-3Nd-0.4Zr) increased to 245 MPa and 150 MPa respectively, especially the elongation increased to 16%. Wang *et al* [19] investigated that the tensile strength and yield strength of both as-cast and aged alloys increase with the increase of Y content. The maximum tensile strength and yield strength of Mg-Nd-Zn-Zr-1.8% Y alloy could reach 198 MPa and 122 MPa at room temperature, respectively. The tensile strength could reach 271 MPa and 161 MPa after peak aging treatment (530 °C/14 h + 200°C/12 h). Comparing with Y-free alloys, it increases by 10.6% and 12.6%, respectively.

The application of magnesium alloys requires not only high strength and toughness, but also good technological properties, especially casting properties. As a result hot tearing susceptibility (HTS) is important especially during solidification, which determines the size and structure complexity of parts or billets [20–29]. So

Table 1. Chemical compositions of experimental alloys (wt)%.

Alloy	Zn	Y	Nd	Mg
Mg-4.5Zn-6Nd	4.5	0	6	Bal.
Mg-4.5Zn-1Y-5Nd	4.5	1	5	Bal.
Mg-4.5Zn-3Y-3Nd	4.5	3	3	Bal.
Mg-4.5Zn-6Y	4.5	6	0	Bal.

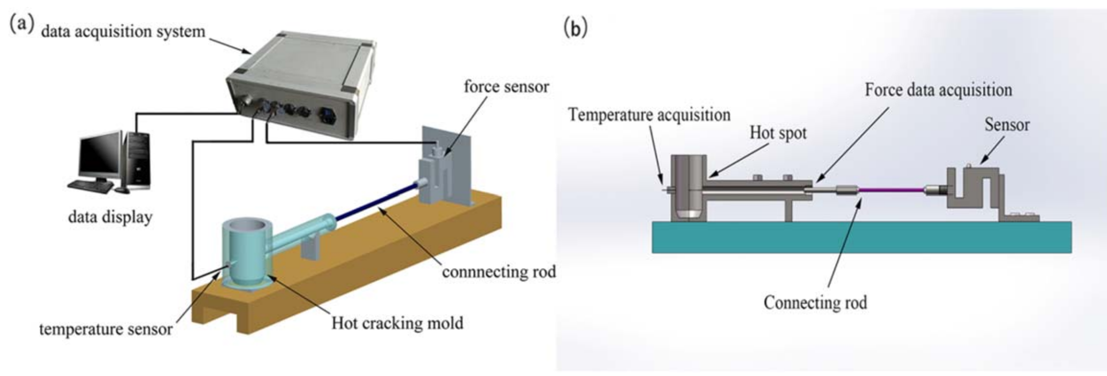

Figure 1. Schematic of experimental setup.

far, about the HTS of Mg-RE-Zn Ternary alloys, Huang *et al* [30] studied the HTS of alloys (Mg-3Nd-0.2Zn-Zr alloys) shows that pouring and mold temperatures significant influence on the HTS and the ranges of pouring and mold temperatures were suggested to be 1003–1033 K and $>=$ 623 K for NZ30K alloy. Liu *et al* [31] studied the HTS systematically of Mg-Y-Zn-Zr alloy shows that MgZn(2.5)Y(1)Zr(0.5) alloy has the lowest hot tearing tendency. However, the HTS of Mg-Y-Nd-Zn alloys with high strength and toughness has not been reported publicly. In this paper, we tried to systematically analyze the hot tearing tendency of Mg-4.5Zn-xY-yNd ($x + y = 6$) alloys. In order to exploit new magnesium alloys with high strength, toughness and low HTS [32–39].

2. Experimental procedure

2.1. Experimental materials and processes

The alloy is made of industrial pure magnesium with a purity of 99.95%, industrial pure zinc with a purity of 99.95%, Mg-25% Y and Mg-20% Nd intermediate alloys as raw materials. First, pure magnesium ingots are melted in stainless steel crucible coated with BN on the inner wall. After melting, pure zinc, magnesium-25% Y and magnesium-20% neodymium master alloys are added in turn. Then, the temperature is adjusted to 700 °C, holding for 40 min, and poured into the preheated die at 280 C. For the preheat treatment of the mold, the whole mold is assembled first, then put into the preheater which is adjusted to 280 °C for at least one hour, and take out when the molten metal is poured. The nominal chemical composition of the refined test alloys is shown in table 1 [40–43].

Hot tearing experiment is used a T-shaped mold. The schematic is shown in figure 1. It is mainly composed of a hot tearing casting system, a sensor and a data acquisition system. The solidification temperature data is collected by a thermocouple inserted into the hot spot. The shrinkage stress acquisition by the sensor through the connecting rod at the end of the mold, and transmitting to analog-to-digital converter (A/D), then displayed in the form of data and charts by computer.

2.2. Double thermocouple analysis system

The solidification curve is collected and analyzed by the double thermocouple analysis system. The schematic diagram is shown in figure 2. Thermocouples are inserted into the center and edge of the crucible to measure the center position temperature (T_c) and the edge position temperature (T_e) during solidification. In order to ensure the heat conduction from the radial direction as much as possible, we use thicker asbestos net seal the top of the crucible. The material used at the bottom is insulating sand and 3 cm thick asbestos to cut heat loss.

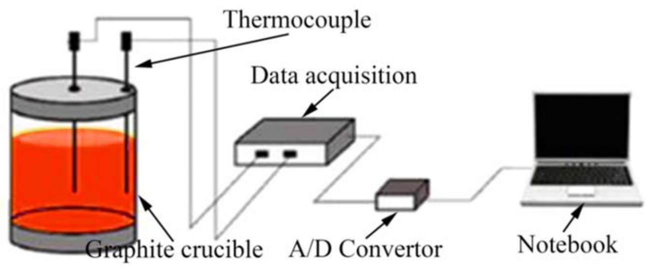

Figure 2. Schematic diagram of double thermocouple test system.

The main purpose of the dual thermocouple analysis system is to determine the dendrite coherence point [44]. The principle as follows: with the decrease of temperature, the solid phase begins to increase continuously. Because the thermal conductivity of solid phase and liquid phase is different, the thermal conductivity of solid phase is larger than that of liquid phase. When dendrites form a continuous network structure, heat diffuses to the edge more easily through the connected solid phase, which reduces the temperature difference between the center and the edge. Therefore, the maximum temperature difference between the central thermocouple and the edge thermocouple indicates that the dendrite begins to coherence. At this time the corresponding temperature of the central thermocouple is the dendrite coherence temperature (T_{coh}).

2.3. Prediction of alloy HTS by clyne-davies model

The prediction of alloy HTS is based on the assumption of Cyne-Davies model [44]. When the solid fraction (f_s) between 0.4 and 0.9, the liquid can be flow freely between dendrites, and the solidification shrinkage can be filled in time. Therefore, the shrinkage stress is fully released without hot tearing, so it is called stress relaxation stage. When the solid fraction higher than 0.9, the dendrites begin to coherence. The residual liquid phase feeding is confined and the feeding mechanism also changes from the whole feeding to the local region feeding between the dendrites. At this time the alloy enters the vulnerable region. As shown in Formula (1), defines the solidification time of f_s between 0.4 and 0.9 as t_R and that of f_s between 0.9 and 0.99 as t_v. The ratio of f_s and f_s is used as a parameter CSC (Cracking susceptibility coefficient) for the determination HTS of alloys. The expression as follows:

$$CSC = \frac{t_V}{t_R} = \frac{t_{0.99} - t_{0.9}}{t_{0.9} - t_{0.4}} \tag{1}$$

$t_{0.99}$ is the time corresponding to $f_s = 0.99$; $t_{0.9}$ is the time corresponding to $f_s = 0.9$; $t_{0.4}$ is the time corresponding to $f_s = 0.4$.

Since the temperature decreases with time monotonously during solidification, the CSC formula can also be expressed in another form, as shown in Formula (2). Here, the temperature difference of solid fraction f_s between 0.4 and 0.9 can be expressed by T_R, between 0.9 and 0.99 can be expressed by T_V [45, 46].

$$CSC* = \frac{T_V}{T_R} = \frac{T_{0.99} - T_{0.9}}{T_{0.9} - T_{0.4}} \tag{2}$$

3. Results and discussion

3.1. Prediction and characterization of alloys HTS by differential thermal analysis

3.1.1. HTS Prediction

Based on the dual-couple temperature curve and the Clyne-Davies model, the calculated CSC and CSC* (Crack Susceptibility Coefficient) of Mg-4.5Zn-xY-yNd ($x + y = 6, x = 0, 1, 3, 6$) alloys are shown in figure 3. The results show that when the total content of rare earth elements is a constant, the HTS depends on the ratio of Y and Nd [31]. The CSC and CSC* of the Mg-4.5Zn-1Y-*x*Nd-0.5Zr alloys are in the following order: Mg-4.5Zn-3Y-3Nd > Mg-4.5Zn-1Y-5Nd > Mg-4.5Zn-6Nd > Mg-4.5Zn-6Y.

3.1.2. Characterization by solidification process

Figure 4 shows the method of double-couple analysis of Mg-4.5Zn-6Y alloy. Under the same cooling conditions, the lower the dendrite coherence temperature (T_{coh}) is, and the larger the solid fraction (f_{coh}) is during coherence, the greater the tendency of hot tearing of alloys.

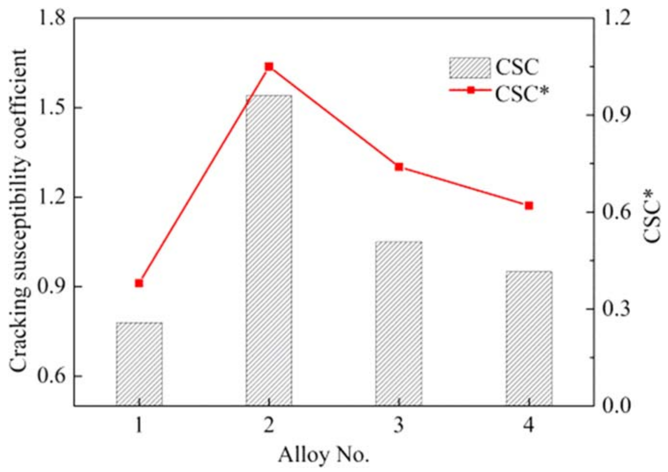

Figure 3. HTS of Mg-4.5Zn-xY-yNd alloys: (1). Mg-4.5Zn-6Y; (2). Mg-4.5Zn-3Y-3Nd; (3). Mg-4.5Zn-1Y-5Nd; 4. Mg-4.5Zn-6Nd.

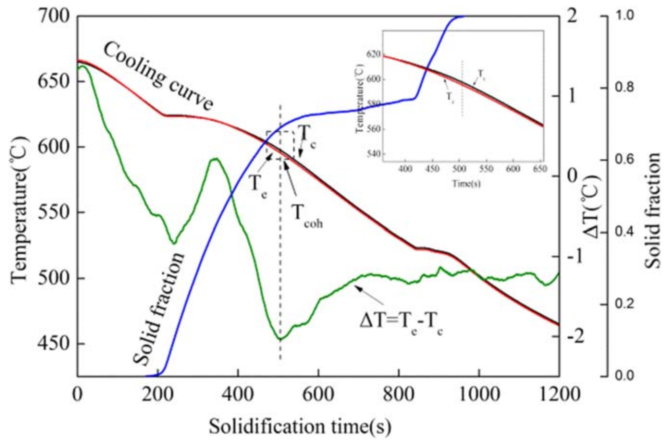

Figure 4. Method of double electric couple analysis of the Mg-4.5Zn-6Y alloy.

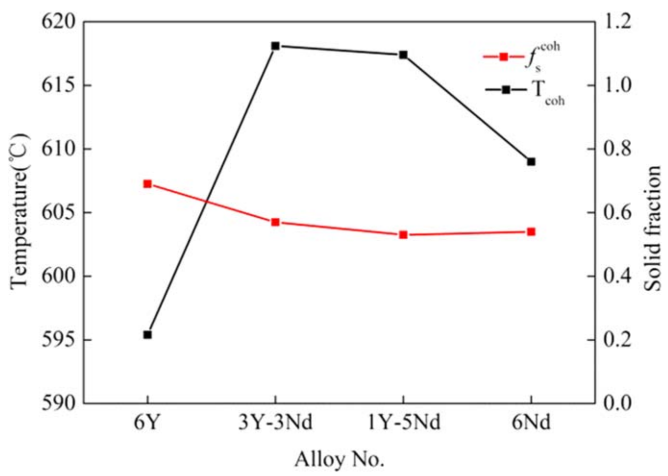

Figure 5. Results of double electric couple analysis of Mg-4.5Zn-xY-yNd alloys.

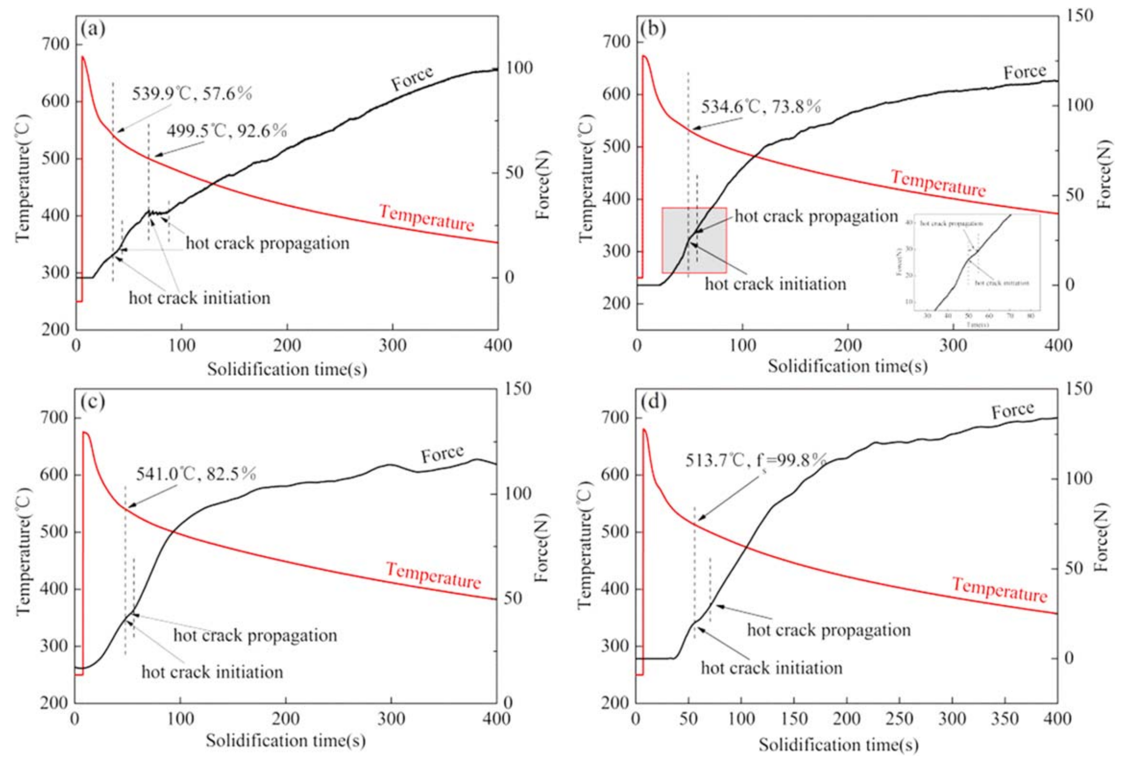

Figure 6. Shrinkage force and temperature as a function of time for Mg-4.5Zn-xY-yNd alloys: (a) Mg-4.5Zn-3Y-3Nd; (b) Mg-4.5Zn-1Y-5Nd; (c) Mg-4.5Zn-6Nd; (d) Mg-4.5Zn-6Y.

Figure 5 is the results of double electric couple analysis of Mg-4.5Zn-xY-yNd alloys. It can be seen that the T_{coh} of the Mg-4.5Zn-6Y alloy is the lowest, and the T_{coh} of the Mg-4.5Zn-3Y-3Nd alloy is the highest, Which may be add two rare earth elements at the same time is more likely to be enriched at the front edge of the solid-liquid interface, and leads to a larger constitutional super-cooling, accelerating dendrite branching and making α-Mg dendrites coherence prematurely. T_{coh} of Mg-4.5Zn-3Y-3Nd, Mg-4.5Zn-1Y-5Nd , Mg-4.5Zn-6Nd and Mg-4.5Zn-6Y alloys are 618.1 °C, 617.4 °C, 609.0 °C and 595.4 °C, respectively, decreasing order of it consistent with CSC*.

3.2. Characterization by temperature-shrinkage stress curve

Figure 6 shows the curve of solidification shrinkage force (F) versus time (t) and the curve of cooling temperature (T) versus time (t) of Mg-4.5Zn-xY-yNd alloys. Corresponding to figures 6(a)–(d), the solid fractions of initial cracking are 57.6%, 73.8%, 82.5% and 99.8%, respectively. As shown in table 3, the initial cracking of Mg-4.5Zn-3Y-3Nd, Mg-4.5Zn-1Y-5Nd, Mg-4.5Zn-6Nd occurs before the precipitation of the second phase, that is to say, the three alloys correspond to the remaining 42.4%, 26.2% and 17.5% liquid phases respectively. In the presence of liquid phase between grains, the strength of grain boundaries is proportional to the surface tension and contact area of liquid phase, and inversely proportional to the thickness of liquid film ($F_{crack} = 2\gamma A/b$. Among them, γ is surface tension of liquid phase, A is contact area between liquid film and matrix, b is the thickness of liquid film). Obviously, the liquid film thickness of Mg-4.5Zn-3Y-3Nd, Mg-4.5Zn-1Y-5Nd, Mg-4.5Zn-6Nd alloys decreases in turn at the initial cracking, which is the main reason for the decrease of their thermal cracking sensitivity.

In addition, for Mg-4.5Zn-6Y alloy, the initial cracking temperature is lower than that of LPSO phase and higher than that of W phase. That is to say, the precipitated LPSO phase will play a role in bridging the two sides of grain boundary to prevent crack growth. Of course, its effect is also related to the nature of LPSO phase itself and the bonding relationship between LPSO phase and matrix crystals.

3.3. Characterization by microstructure evolution

Figure 7 shows the as-cast microstructure and precipitated second phase morphology of Mg-4.5Zn-xY-yNd alloys. Figure 8 shows the XRD diffraction patterns of Mg-4.5Zn-xY-yNd alloys. It can be seen that the main precipitated phase of the Mg-4.5Zn-6Y alloy is the LPSO phase ($Mg_{12}ZnY$), the main precipitated phase of the Mg-4.5Zn-3Y-3Nd and Mg-4.5Zn-1Y-5Nd alloy is W-phase ($Mg_3Zn_3(Y,Nd)_2$),and the main precipitation of Mg-4.5Zn-6Nd alloy is T-phase (Mg-Zn-Nd ternary phase). Moreover, the morphology of W-phase and

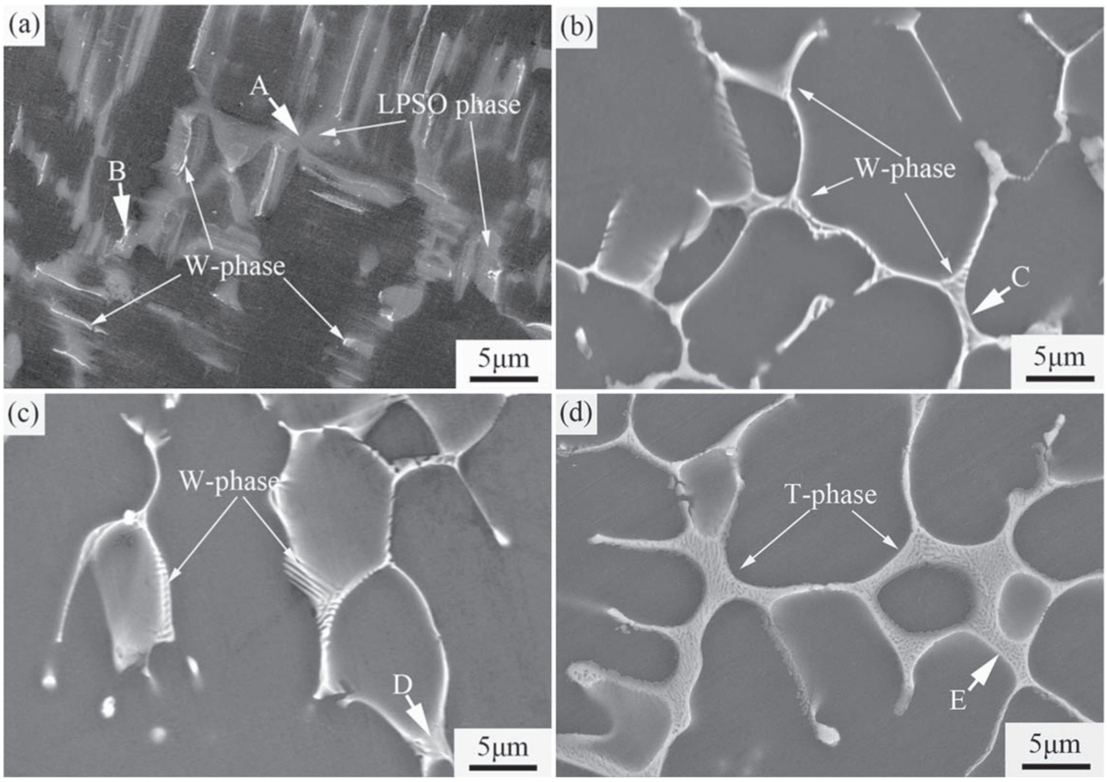

Figure 7. SEM images of Mg-4.5Zn-xY-yNd alloys: (a) Mg-4.5Zn-6Y; (b) Mg-4.5Zn-3Y-3Nd; (c) Mg-4.5Zn-1Y-5Nd; (d) Mg-4.5Zn-6Nd.

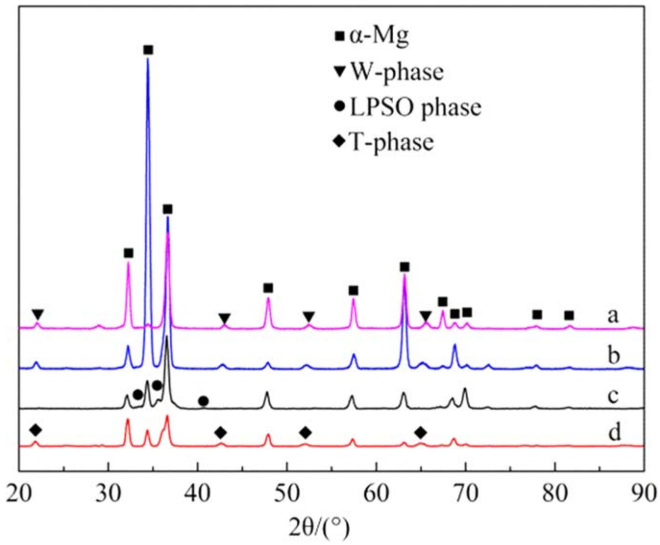

Figure 8. XRD spectra of Mg-4.5Zn-xY-yNd alloys: (a) Mg-4.5Zn-3Y-3Nd; (b) Mg-4.5Zn-1Y-5Nd; (c) Mg-4.5Zn-6Y; (d) Mg-4.5Zn-6Nd.

T-phase shows a network structure along grain boundaries, while LPSO phase tends to extend from grain boundary to intragranular direction [47].

The composition of the low melting eutectic phase analyzed by EDS is shown in table 2. LPSO phase is the main low melting precipitation and a small amount of W-phase ($Mg_3Zn_3Y_2$) without adding Nd. With the change of Y and Nd ratio, LPSO phase disappeared and $Mg_3Zn_3Y_2$ transformed into $Mg_3Zn_3(Y,Nd)_2$. The main precipitation is T-phase without Y.

Transmission electron microscope (TEM) patterns of the LPSO phase and W-phase in figures 9(a) and (b), respectively. The LPSO phase is precipitated by eutectic reaction of residual liquid at 544.7°C, and the atomic

Table 2. The EDS results of the second phase marked by the white arrows and letters in figure 4 Mg-4.5Zn-xY-yNd alloys.

	Chemical compositions (at%)				
Position	Mg	Zn	Y	Nd	Phase
A	80.23	16.81	2.96	—	LPSO phase
B	69.85	26.63	3.52	—	W-phase($Mg_3Zn_3Y_2$)
C	74.91	21.63	0.86	2.60	W-phase $Mg_3Zn_3(Y, Nd)_2$
D	72.49	20.28	1.28	5.96	W-phase $Mg_3Zn_3(Y, Nd)_2$
E	64.04	26.41	—	9.55	T-phase

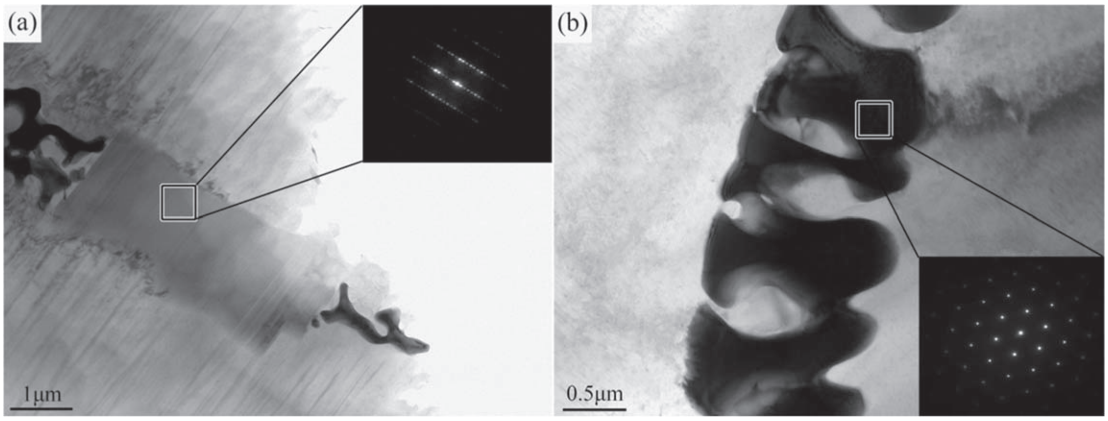

Figure 9. TEM patterns of the Mg-Zn-Y LPSO-phase and W-phase.

stacking is similar to that of a-Mg phase with stacking faults. The distribution of rare earth and zinc atoms is periodically distributed on stacking faults. Although the lattice constants are different, there is still a certain coherent relationship between the two phases. Moreover, the strength of the precipitated LPSO phase has a strong pinning force on both sides of grain boundary of a-Mg.

3.4. Characterization by Fracture Morphology

Figure 10 shows the fracture morphology of Mg-4.5Zn-xY-yNd alloys. The tearing liquid film of Mg-4.5Zn-3Y-3Nd alloy has thick wrinkles and stretched 'Wiredrawing' on the fracture surface in figure 10(a). According to the and F-t curves of Mg-4.5Zn-3Y-3Nd, the first hot tearing initiation at the temperature of 539.9°C and solid fraction is 57.6%, Because there are still more liquid phase remaining at this time, the crack is fully fed. However, the solidification shrinkage stress increases further during solidification, and the second crack forms at the temperature of 499.5°C ($f_s = 92.6\%$), the feeding position is stretched again. indicating that Mg-4.5Zn-3Y-3Nd alloy has high HTS. Figures 10(b), (c) shows that the folded liquid film obvious decrease compared with figure 10(a), indicating that the liquid fraction is low and the crack initiation is late relatively. The low melting phase can fed the crack and reduce the tendency of hot tearing to some extent. This is consistent with the analysis of the temperature-stress curve, so these two alloys have low HTS than the alloy of figure 10(a). By observing the thickness and continuity of the tear film, As shown in figure 10(d), it is caused by minute cracks initiation at the end of the solidification. At this time, the strength of the alloy is close to the maximum, and the crack is difficult to propagation, so the hot tearing resistance is the best.

3.5. Characterization by thermal analysis curve

Figure 11 shows the cooling curve, first derivative curve and baseline determined by Newton baseline method of Mg-4.5Zn-xY-yNd alloys. When there is inflection point in the cooling curve and exothermic peak in the first derivative curve of temperature, it indicates that the latent heat of crystallization is released and a new phase is precipitated in the liquid phase. The temperatures of each precipitation in the figure 11 are shown in table 3.

It can be seen from figure 11 and table 3 that the latent heat peak and precipitation temperature of the second phase of Mg-4.5Zn-3Y-3Nd alloy, Mg-4.5Zn-1Y-5Nd alloy, Mg-4.5Zn-6Nd alloy and Mg-4.5Zn-6Y alloy increase in turn, which indicates that the residual liquid phase between the dendrites increases sequentially after the precipitation of the α-Mg phase. As a result, not only the feeding capacity of the residual liquid phase

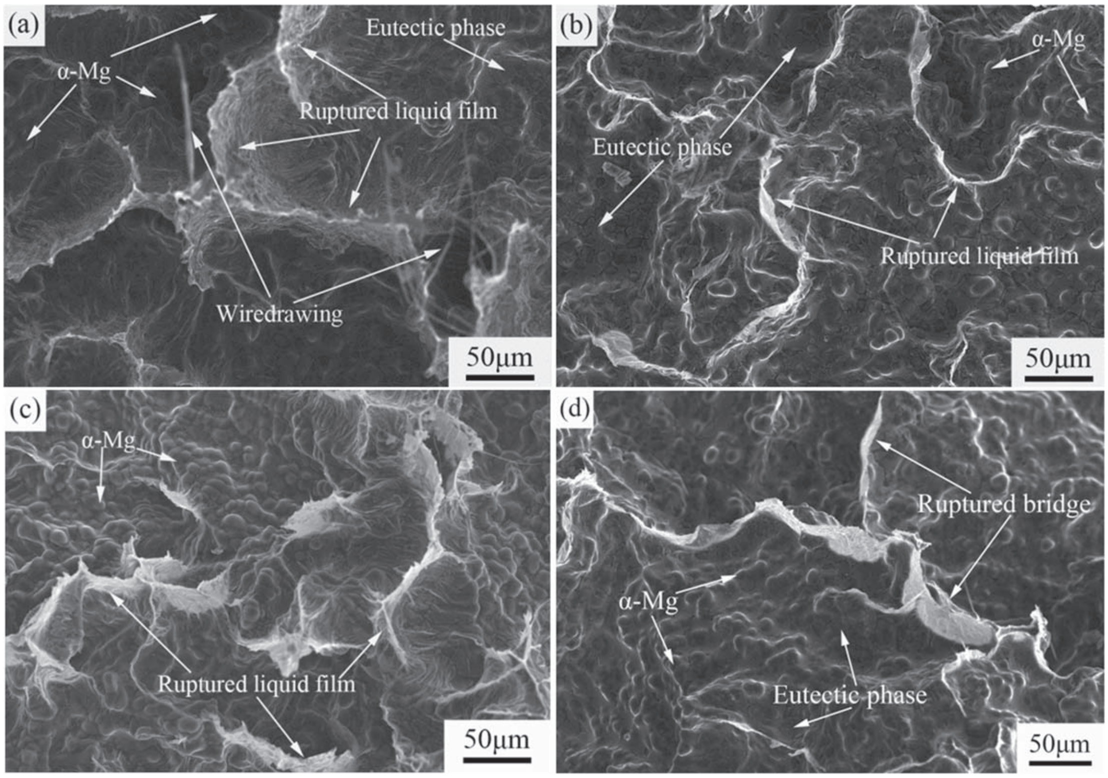

Figure 10. Fracture morphologies of Mg-4.5Zn-xY-yNd alloys: (a) Mg-4.5Zn-3Y-3Nd; (b) Mg-4.5Zn-1Y-5Nd; (c) Mg-4.5Zn-6Nd; (d) Mg-4.5Zn-6Y.

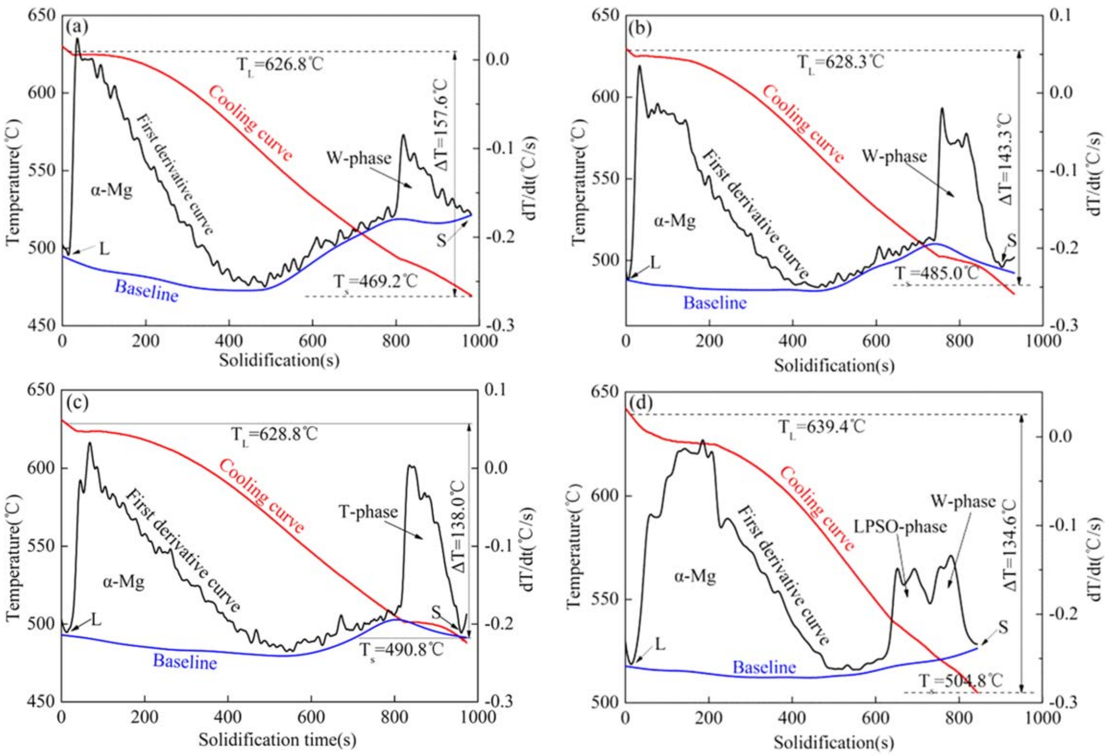

Figure 11. Solidification path of Mg-4.5Zn-xY-yNd alloys: (a) Mg-4.5Zn-3Y-3Nd; (b) Mg-4.5Zn-1Y-5Nd (c); Mg-4.5Zn-6Nd; (d) Mg-4.5Zn-6Y.

Table 3. Thermal analysis results for the characteristic temperatures for Mg-4.5Zn-xY-yNd alloys.

Alloy	α-Mg	LPSO phase	W-phase	T-phase	T_S
Mg-4.5Zn-3Y-3Nd	626.8 °C	—	496.4 °C	—	469.2 °C
Mg-4.5Zn-1Y-5Nd	628.3 °C	—	504.7 °C	—	485.0 °C
Mg-4.5Zn-6Nd	628.8 °C	—	—	505.8 °C	490.8 °C
Mg-4.5Zn-6Y	631.9 °C	544.7 °C	525.4° C	—	504.8 °C

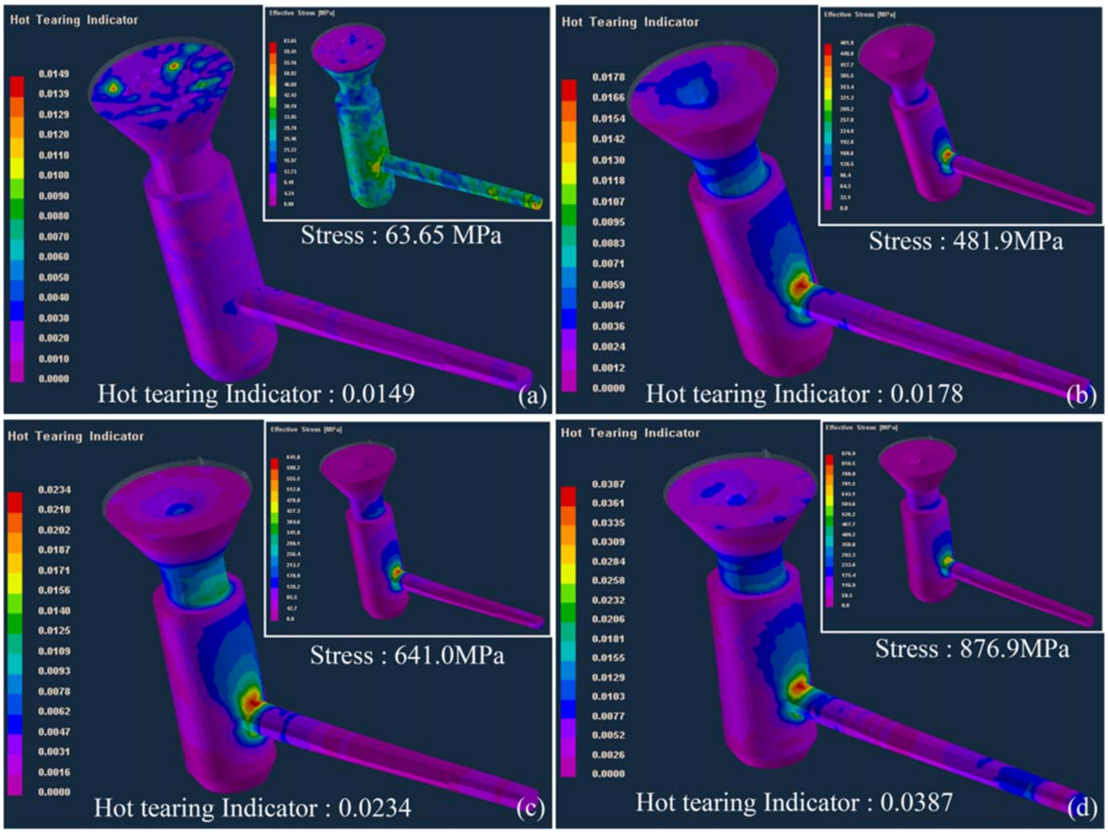

Figure 12. Comparison between HTI predicted and the distribution of stress using ProCAST of Mg-4.5Zn-xY-yNd alloys at mold temperature of 280°C: (a) Mg-4.5Zn-6Y; (b) Mg-4.5Zn-6Nd; (c) Mg-4.5Zn-1Y-5Nd; (d) Mg-4.5Zn-3Y-3Nd.

between the dendrites is improved, but also the local temperature rise between the dendrites is increased to relieve the solidification shrinkage stress and reduce the HTS of the alloy.

3.6. Numerical simulation of HTS

Figure 12 shows the calculated Hot Tearing Indicator (HTI) and Stress at the hot spot for Mg-4.5Zn-xY-yNd alloys. HTI provide a good indication for the susceptibility of the hot tearing occurred during solidification. The simulation results show that the hot tearing tendency of Mg-4.5Zn-6Y alloy, as shown in figure 12(a), is obviously different from that of the other three alloys. Its HTI value is the smallest and stress distribution at the hot spot is more uniform. When the ratio of Nd is 3%, the HTS is the highest. The susceptibility of hot tearing predicted by numerical simulation is in good agreement with that obtained by experimental observations.

4. Conclusion

(1) When the total content of (Y + Nd) in the alloy is constant (6 wt%), the predicted and measured HTS of Mg-4.5Zn-xY-yNd alloys changes with the relative content of Y and Nd. The order from high to low is Mg-4.5Zn-3Y-3Nd, Mg-4.5Zn-1Y-5Nd, Mg-4.5Zn-6Nd, Mg-4.5Zn-6Nd and Mg-4.5Zn-6Y.

(2) The precipitations have an important effect on the hot tearing tendency of Mg-4.5Zn-xY-yNd alloys. The latent heat peak and precipitation temperature of the second phase of Mg-4.5Zn-3Y-3Nd alloy, Mg-4.5Zn-1Y-5Nd alloy, Mg-4.5Zn-6Nd alloy and Mg-4.5Zn-6Y alloy increase sequentially, which not only improves

the feeding capacity of the residual liquid phase between dendrites, but also increases the local temperature between dendrites to alleviate the solidification shrinkage stress and reduce the HTS of the alloys.

(3) According to the fracture temperature and solid fraction of the alloys, hot tearing occurs in the middle and late solidification stages, and the interdendritic liquid phase and its crystallization behavior have a great influence on the hot tearing. The residual liquid phase with eutectic composition feeding and the coherent extension of the second phase precipitated at high temperature to the matrix can effectively pin grain boundaries and inhibit the nucleation and growth of hot cracks.

Acknowledgments

This work is supported by the National Natural Science Foundation of China (Grant No.51571145) and Ningbo Science and Technology Innovation 2025 Major Project (Project name: Research on precision forming technology of new energy automobile lightweight magnesium alloy material).

Disclosure statement

No potential conflict of interest is reported by the authors.

ORCID iDs

Xingxing Li https://orcid.org/0000-0001-8470-5371
Yue Wang https://orcid.org/0000-0002-7272-7589
Ziqi Wei https://orcid.org/0000-0002-9883-0269

References

[1] Tahreen N and Chen D L 2016 A critical review of Mg-Zn-Y series alloys containing I, W, and LPSO phases *Adv. Eng. Mater.* **18** 1983–2002
[2] Wang Z, Huang Y D, Srinivasan A, Liu Z, Beckmann F and Kainer K U 2014 Experiment and numerical analysis of HTS for Mg-Y alloys *J. Mater. Sci.* **49** 353–62
[3] Zhou Z J, Liu Z, Wang Y, Mao P L, TangWR and Zhou Y 2018 Investigations on the effect of grain size on HTS of $MgZn_1Y_2$ alloy *Mater. Res. Express* **5** 056511
[4] Gunde P, Schiffl A and Uggowitzer P J 2010 Influence of yttrium additions on the HTS of magnesium-zinc alloys *Mater. Sci. Eng.* A **527** 7074–9
[5] Sravya T, Sankaranarayanan S, Abdulhakim A and Manoj G 2015 Mechanical properties of magnesium-rare earth alloy systems: a review *Metals* **5** 1–39
[6] Bita P, Hamed M and Massoud E 2017 Toward unraveling the effects of intermetallic compounds on the microstructure and mechanical properties of Mg–Gd–Al–Zn magnesium alloys in the as-cast, homogenized, and extruded conditions *Mater. Sci. Eng.* A **680** 39–46
[7] Jiang Z, Jiang B and Zeng Y 2015 Role of Al modification on the microstructure and mechanical properties of as-cast mg-6Ce alloys *Mater. Sci. Eng.* A **349** 207–12
[8] Wu G, Yu F and Hong T G 2005 The effect of Ca and rare earth elements on the microstructure, mechanical properties and corrosion behavior of AZ91D *Mater. Sci. Eng.* A **408** 255–63
[9] Bita P, Hamed M and Massoud E 2018 The effects of grain refinement and RareEarth intermetallics on mechanical properties of as-cast and wrought magnesium alloys *J. Mater. Eng. Perform.* **27** 1327–33
[10] Yu H, Hong G Y and Chen J H 2014 Effects of minor Gd addition on microstructures and mechanical properties of the high strain-rate rolled Mg–Zn–Zr alloys *J. Alloys Compd.* **58** 757–65
[11] Roostaei M, Parsa M H and Mahmudi R 2015 Hot compression behavior of GZ31 magnesium alloy *J. Alloys Compd.* **631** 1–6
[12] Bu F, Qiang Y and Kai G 2016 Study on the mutual effect of La and Gd on microstructure and mechanical properties of Mg-Al-Zn extruded alloy *J. Alloys Compd.* **688** 1241–50
[13] Mirzadeh H, Roostaei M and Parsa M H 2015 Rate controlling mechanisms during hot deformation of Mg–3Gd–1Zn magnesium alloy: dislocation glide and climb, dynamic recrystallization, and mechanical twinning *Mater Design* **68** 228–31
[14] Wang M, Zhou H and Wang L 2007 Effect of yttrium and cerium addition on microstructure and mechanical properties of AM50 magnesium alloy *J. Rare. Earth* **25** 233–7
[15] Liu X B, Chen R S and Han E H 2008 Effects of ageing treatment on microstructures and properties of Mg–Gd–Y–Zr alloys with and without Zn additions *J. Alloys Compd.* **465** 232–8
[16] Liu Q, Ding X and Liu Y 2017 Analysis on micro-structure and mechanical properties of Mg-Gd-Y-Nd-Zr alloy and its reinforcement mechanism *J. Alloys Compd.* **690** 961–5
[17] Chang J W *et al* 2007 Effect of heat treatment on corrosion and electrochemical behavior of Mg-3Nd-0.2Zn-0.4Zr(wt%) alloy *Electrochim. Acta.* **52** 3160–7
[18] Fu P *et al* 2008 Effects of heat treatments on the microstructures and mechanical properties of Mg-3Nd-0.2Zn-0.4Zr(wt%) alloy *Mater. Sci. Eng.* A **486** 183–92
[19] Gao Y *et al* 2010 Electroless nickel plating on ZM6 (Mg-2.6Nd-0.6Zn-0.8Zr) magnesium alloy substrate *Surf. Coat. Technol.* **204** 3629–35

[20] Davis T A *et al* 2018 Effect of TiBor on the grain refinement and HTS of AZ91D magnesium alloy *J. Alloys Compd.* **759** 70–79
[21] Clyne T W and Davies G J 1981 The influence of compositon on solidification cracking susceptibility in binary alloys *Br. Foundryman* **74** 65–73
[22] Zhou L *et al* 2012 Prediction of HTS for Mg-Zn-(Al) alloys *Adv. Mater. Res.* **509** 138–46
[23] Wang Z *et al* 2016 HTS of Mg-xZn-2Y alloys *Trans. Nonferrous. Metal. Soc. China* **26** 3115–22
[24] Liu J *et al* 2017 A novel biodegradable and biologically functional Arginine-based poly (ester urea urethane) coating for Mg-Zn-Y-Nd alloy: enhancement in corrosion-resistance and biocompatibility *J. Mater. Chem.* B **5** 1787–802
[25] Wei Z Q *et al* 2018 Effects of Zn and Y on hot-tearing susceptibility of Mg-*x*Zn-2*x*Y alloys *Mater. Sci. Technol.* **34** 2001–7
[26] Sanjari M *et al* 2017 The role of the Zn/Nd ratio in the microstructural evolution of the Mg-Zn-Nd system during static recrystallization: Grain boundary partitioning of solutes *Scripta. Mater.* **134** 1–5
[27] Du B N *et al* 2018 Influence of Zn Content on Microstructure and Tensile Properties of Mg-Zn-Y-Nd Alloy *Acta. Metall. Sin. (Engl. Lett.)* **31** 1–11
[28] Wen L, Ji Z and Li X 2008 Effect of extrusion ratio on microstructure and mechanical properties of Mg-Nd-Zn-Zr alloys prepared by a solid recycling process *Mater. Charact.* **59** 1655–60
[29] Qiang L *et al* 2013 Effect of Nd and Y addition on microstructure and mechanical properties of as-cast Mg-Zn-Zr alloy *Alloys. Compd.* **588** 97–102
[30] Huang H *et al* 2014 Effect of pouring and mold temperatures on HTS of AZ91D and Mg-3Nd-0.2Zn-Zr Mg alloys *Trans. Nonferrous. Metal. Soc. China* **24** 922–9
[31] Liu Z *et al* 2014 Effects of Y on HTS of Mg-Zn-Y-Zr alloys Trans *Nonferrous. Metal. Soc. China* **24** 907–14
[32] Wang Z *et al* 2016 Effect of Cu additions on microstructure, mechanical properties and hot-tearing susceptibility of Mg-6Zn-0.6Zr Alloys *J. Mater. Eng. Perform.* **25** 5530–9
[33] Luo S Q *et al* 2011 Effect of mole ratio of Y to Zn on phase constituent of Mg-Zn-Zr-Y alloys *Tran. Nonferr. Met. Soc. China* **21** 795–800
[34] Bichler L and Ravindran C 2015 Investigations on the stress and strain evolution in AZ91D magnesium alloy castings during hot tearing *J. Mater. Eng. Perform.* **24** 2208–18
[35] Xie J C *et al* 2008 Microstructure and mechanical properties of AZ81 magnesium alloy with Y and Nd elements *Trans. Nonferrous Met. Soc. China* **18** 303–8
[36] Xu D K *et al* 2007 Effect of Y Concentration on the Microstructure and Mechanical Properties of as-cast Mg-Zn-Y-Zr alloys *J. Alloys Compd.* **432** 129–34
[37] Song J F *et al* 2016 Hot tearing characteristics of Mg-2Ca-xZn alloys *J. Mater. Sci.* **51** 2687–704
[38] Zhu Y *et al* 2004 Effects of yttrium on microstructure and mechanical properties of hot-extruded Mg-Zn-Y-Zr alloys *Mater. Sci. Eng.* A **373** 320–7
[39] Wang Z *et al* 2013 HTS of binary Mg-Y alloy castings *Mater. Des.* **47** 90–100
[40] Hao H *et al* 2010 Modeling the stress-strain behavior and hot tearing during direct chill casting of an AZ31 magnesium billet *Metall. Mater. Trans.* A **41** 2067–77
[41] Cao G, Haygood I and Kou S 2010 Onset of hot tearing in ternary Mg-Al-Sr alloy castings *Metall. Mater. Trans.* A **41** 2139–50
[42] Clyne T W, Wolf M and Kurz W 1982 The effect of melt composition on solidification cracking of steel, with particular reference to continuous casting *Metall. Trans.* B **13** 259–66
[43] Kou S 2015 A criterion for cracking during solidification *Acta Mater.* **88** 366–74
[44] Srinivasan A *et al* 2013 Hot tearing characteristics of binary Mg-Gd alloy castings *Metall. Mater. Trans.* A **44** 2285–98
[45] Bichler L, Ravindran C and Sediako D 2008 Neutron diffraction measurement of strain required for the onset of hot tearing in AZ91D magnesium alloy *T. Indian. I. Metals* **61** 293–300
[46] Beals R S *et al* 2007 USAMP magnesium powertrain cast components: fundamental research summary *JOM* **59** 43–8
[47] Zhou Z *et al* 2018 Effects of the second phase on HTS of Mg-Zn-Y alloy *Mater. Res. Express* **6** 2053–1591
[48] Cao G and Kou S 2006 Hot tearing of ternary Mg-Al-Ca alloy castings *Metall. Mater. Trans.* A **37** 3647–63